Article

Radiation Shielding Property of Concrete Using Electric Arc Furnace Oxidizing Slag Aggregate

Han-Seung Lee[1], Hee-Seob Lim[1]*, Jae-Seok Choi[2]

Received: date; Accepted: date; Published: date
Academic Editor: name

1 Department of Architecture Engineering, Hanyang University, 55, Hanyangdaehak-ro, Sangrok-gu, Ansan-si, Gyeonggi-do 15588, Korea; ercleehs@hanyang.ac.kr
2 Korea Conformity Laboratories, 199, Gasan difital 1-ro, Geumcheon-gu, Seoul, 08503, Korea; choijs@kcl.re.kr
* Correspondence: heesubjm@naver.com; Tel.: +82-31-400-5181; Fax:+82-31-436-8169

Abstract: Electric arc furnace oxidizing slag (EAF) has a high density of 3.0~3.7 t/m^3 and therefore has a high bulk density when mixed with concrete. Extensive research has been conducted on the use of concrete with high unit volume weight as heavyweight concrete for radiation shielding concrete. In this study, to examine the possibility of developing a radiation shielding concrete, the physical properties of normal concrete, magnetite concrete, EAF concrete, and EAF concrete with added iron powder, were compared. Also, their radiation shielding performance was assessed through shielding tests against X-rays and γ-rays. While the unit volume weight of EAF concrete (3.21 t/m^3) appeared lower than that of magnetite concrete (3.5 t/m^3), the compressive strength of EAF concrete was greater than those of magnetite and normal concretes. The radiation shielding ratio of magnetite concrete was observed to be 93.9% from the X-ray shielding test, followed by 91.2% of EAF concrete, and 73.7% of normal concrete, indicating a linear relationship with unit volume weight. From the γ-ray shielding test, the performance of EAF and magnetite concretes appeared to be similar. Based on the excellent physical properties and radiation shielding performance of EAF concrete, its potential applicability as radiation shielding concrete was confirmed.

Keywords: steel slag; electric arc furnace slag; magnetite; radiation shielding concrete; concrete; EAF; aggregate

1. Introduction

Radiation shielding concretes are commonly used in nuclear power plants, nuclear medicine facilities, and nuclear research facilities [1- 5]. With respect to the material for production of radiation shielding concretes, the guidelines in ACI 304R specify that magnetite, barite, and hematite in high ratios and colemanite and boron additives in low ratios should be used as the materials for the production of radiation shielding concretes. The guidelines from the International Commission on Radiological Protection (ICRP) are widely used as the standard for radiation shielding [6]. While materials with high-specific gravity are required for the shielding of gamma rays, materials such as water, boron, and graphite can be used for neutron radiation [7]. The radiation shielding property varies with the amount and type of concrete aggregates [8, 9]. Although magnetite or barite (density greater than 4.0 t/m^3) have been used in previous studies [10, 11], they involve numerous problems pertaining to concrete manufacturing, such as low slump, low compressive strength, and material segregation of concrete. Various materials have been used in previous studies to alleviate these issues and develop radiation shielding concrete [12]. For example, research has been conducted on the development of concrete based on radiation shielding materials such as lead and iron [13- 15]. There have been studies on the effect of adding silica fume and blast furnace slag [16] on the

Preprints (www.preprints.org) | NOT PEER-REVIEWED | Posted: 4 October 2016 doi: 10.20944/preprints201610.0006.v1

attenuation coefficient [17], and a study on the development of radiation shielding concrete based on the aggregates specific to each nation (e.g., stones or soil) [18, 19]. Much research has been conducted on high-density aggregates [20]. A few recent studies have focused on steel industry by-products [21, 22]. Although these by-products contain a large amount of recyclable and useful resources, current measures of disposal rely primarily on depositing them into landfills. With global attention to environmental problems, the practical applicability of industrial by-products is being researched [23]. Among steel slags, extensive research has been conducted on the recyclability of electric arc furnace (EAF) oxidizing slag [24]. While the use of EAF oxidizing slag is increasing with global advances in the steel industry, it is only used in road base and subbase, or hot mix asphalt, and is otherwise deposited in landfills, and no clear recycled use is known [25]. Research has been conducted to assess the possibility of developing concrete based on EAF oxidizing slag aggregates (EAF), the improvement effect of concrete on compressive strength, and the enhancement of durability [26- 28]. EAF oxidizing slag contains iron (15 – 30%), and has a high density of 3.0-3.7 t/m^3. Therefore, it is believed that such high-density EAF can be used as an aggregate for radiation shielding concrete.

In this study, the possibility of developing a radiation shielding concrete through radiation shielding test of magnetite-based concrete and EAF concrete was verified by reviewing the physical and chemical properties of EAF, which is an industrial byproduct, and assess the radiation shielding performance of concretes based on each material through X-ray and γ-ray irradiation experiments.

2. Experimental

2.1 Materials

Normal aggregates, EAF, magnetite, and iron powder were used, and experiments were conducted to measure the physical properties of the aggregates that were specified by ASTM C 33 [29], ASTM C 29 [30], ASTM C 127 [31], ASTM C 128 [32], and ASTM C 136 [33]. Table 1 shows the mechanical properties of the used materials.

Table 1. Mechanical properties of used materials

Material		Physical properties
Cement		OPC (density : 3.14 t/m^3)
Fine aggregates	Washed river sand	density : 2.61 t/m^3, Fineness Modulus : 2.69, absorption : 1.32%
	EAF 1	density : 3.70 t/m^3, Fineness Modulus : 2.71, absorption : 1.10%
	EAF 2	density : 3.38 t/m^3, Fineness Modulus : 2.54, absorption : 2.00%
	Magnetite	density : 4.30 t/m^3, Fineness Modulus : 2.75, absorption : 0.61%
	Iron powder	density : 7.20 t/m^3, absorption : 0.10%
Coarse aggregates	Crushed granites	density : 2.62 t/m^3, Fineness Modulus : 6.86, absorption : 0.80%
	EAF 1	density : 3.78 t/m^3, Fineness Modulus : 6.62, absorption : 1.34%
	EAF 2	density : 3.42 t/m^3, Fineness Modulus : 6.36, absorption : 2.72%
	Magnetite	density : 4.40 t/m^3, Fineness Modulus : 6.80, absorption : 0.50%
Super plasticizer		Poly carboxylate ether (density : 1.05 t/m^3)

doi: 10.20944/preprints201610.0006.v1

Ordinary Portland cement (OPC), specified by ASTM C 150-05 [34], was used. EAFs have varying density depending on the steelmaking process. The unit volume weights of EAF1 and EAF2 are 3.7 t/m³ and 3.4 t/m³, respectively. The density of magnetite is over 4.3 t/m³, and its fitness modulus (FM) was adjusted discretionarily to suffice for its use as a concrete aggregate during the experiment. Figures 1 and 2 show the grading curves for aggregates.

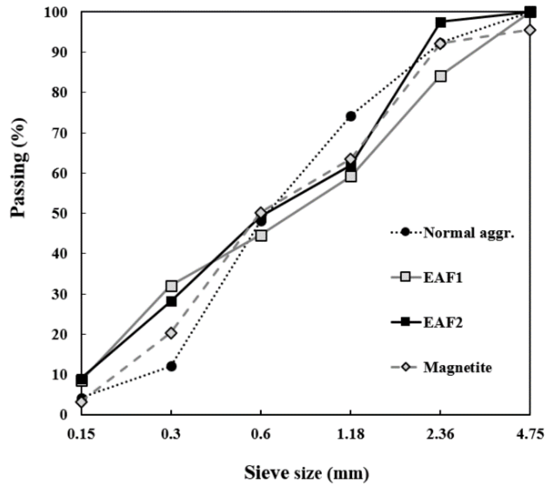

Figure 1. Grading curves for fine aggregates (ASTM C 136)

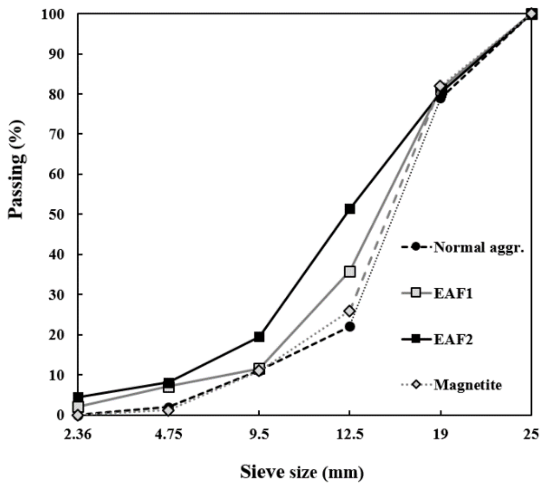

Figure 2. Grading curves for coarse aggregates (ASTM C 136)

In order to obtain a radiation shielding ratio similar to that of previous radiation shielding concretes using EAF, iron powder was used in this study. The iron powder was generated as an industrial byproduct of the steelmaking process. Iron powder has a high density of around 7.2 t/m³, and comprises more than 90 % Fe_2O_3.

Table 2 shows the chemical composition of each material determined by XRF analysis. EAF contains around 35 % iron and therefore has a high density. Thus, it is believed that the use of EAF for radiation-shielding concretes in place of normal aggregates will be highly effective.

Table 2. Chemical properties of the materials (mass ratio, %)

	Fe_2O_3	CaO	SiO_2	Al_2O_3	MnO	MgO	SO_3	TiO_2	etc.
OPC	3	62	22	5	-	3	3	-	2
EAF1	37	26	15	11	6	3	-	-	2

EAF2	35	20	20	9	7	5	-	-	4
Magnetite	58	2	10	5	-	5	-	17	3
Iron Powder	92	-	-	-	-	-	-	-	8

-: not provided; Etc. shows the ZnO, K_2O, P_2O_5, Na_2O

2.2 Experimental Plan

The mix design was based on water/cement (W/C) ratios of 0.4 and 0.45, and the concrete had a W/C ratio of 0.45. Iron powder, the amount of which was calculated using Equation (1), was discretionarily added to increase the unit volume weight. To utilize Equation (1), the volumetric contents in unit volume are calculated using Equation (2), and the weights of both coarse and fine aggregates are calculated using Equations (3) and (4) respectively. The weight of cement is calculated using Equation (5). After calculating the unit volume weight of each material, the unit volume weight of each concrete was calculated based on the concrete mix design, and iron powder was added at a unit volume weight over 3.4 t/m³. During the mixing of magnetite concretes with W/C ratios of 0.4 and 0.45, the admixture content was increased; this is because the densities of the fine particles of magnetite and the magnetite itself are high. Two different types of EAF; EAF1 and EAF2, with different physical properties were used. Table 3 shows the mix design used for the experiment.

$$\text{Unit weight}(kg/m^3) = W + C + G + S \tag{1}$$

$$\mathrm{V} = 1000 - (W + C_v + air) \tag{2}$$

$$\mathrm{G} = \mathrm{V} \times \left(\frac{100 - S/a}{100}\right) \times G_d \tag{3}$$

$$\mathrm{S} = \mathrm{V} \times \left(\frac{\mathrm{S/a}}{100}\right) \times S_d \tag{4}$$

$$C_v = \frac{\boldsymbol{C}}{cement's\ density(= 3.14)} \tag{5}$$

Where, V is the volume of the aggregates
G = weight of the coarse aggregates
G_d = density of the coarse aggregates
S = weight of the fine aggregates
S_d = density of the fine aggregates
C = weight of the cement
C_v = volumetric of the cement
W = weight of the water
S/a = fine aggregates modulus

Table 3. Mix design (kg/m³)

Symbol of specimen	W/C ratio	S/A (%)	W	C	Fine aggregate					Coarse aggregate				Ad.
					NF	EAF 1	EAF 2	MA.	Ir.	NC	EAF 1	EAF 2	MA.	
40N	0.40	49	165	413	868		-		-	911	-	-	-	3.3
40E(1)					-	1257	-	-	-	-	1308	-	-	3.3

40M					-	-	-	1508	-	-	-	-	1570	4.1
40E(1)M					-	1257	-	-	-	-	-	-	1570	3.3
45N	0.45	47	180	400	844	-	-	-	-	959	-	-	-	3.3
45E(1)					-	1186	-	-	-	-	1338	-	-	3.3
45E(2)					-	-	1069	-	-	-	-	1220	-	3.3
45M					-	-	-	1423	-	-	-	-	1605	4.0
45E(1)M -Ir(10%)					-	1199	-	-	133	-	-	-	1686	3.3
45E(1)-Ir (40%)					-	997	-	-	665	-	1387	-	-	3.3

-: not provided

NF: Natural fine aggregates (Sand), NC: Natural coarse aggregates (Granite), EAF: Electric Arc Furnace Oxidizing Slag, Ir.: Iron powder, MA.: Magnetite, Ad.: Super plasticizer

Normal aggregates, magnetite, and EAF were used. For fresh concrete, the air content and unit volume weight were measured using ASTM C 173 [35], and a slump test was conducted using ASTM C 143 [36]. With hardened concrete, ASTM C 39 [37] compressive strength tests, X-ray irradiation experiments, and gamma-ray irradiation experiments were conducted. The unit volume weight of hardened concrete was calculated as the average of three cylinder specimens of dimensions Ø10 ×20 cm after standard curing. The specimens for X-ray and γ-ray irradiation experiments had dimensions of 13.6 × 16 × 5 cm; specimens with dimensions of Ø10 ×20 cm were cured for 3, 7, and 28 days and used for compressive strength tests.

2.3 Experimental Methods and Measurement Items

Figure 3 shows the X-ray irradiation experiment. The X-ray from the X-ray generator is attenuated by each specimen, and the dosage is calculated using the LaBr3(Ce) detector. The distance between the X-ray generator and the specimen was kept constant at 1 m for all specimens, and the thickness of all the specimens was 5 cm. Specimens with dimensions of 13.6 × 16 × 5 cm were manufactured and a LaBr3(Ce) scintillator detector was used. The X-ray spectrum was generated at a voltage of 150 kVp. Table 4 show the description of the X-ray generator.

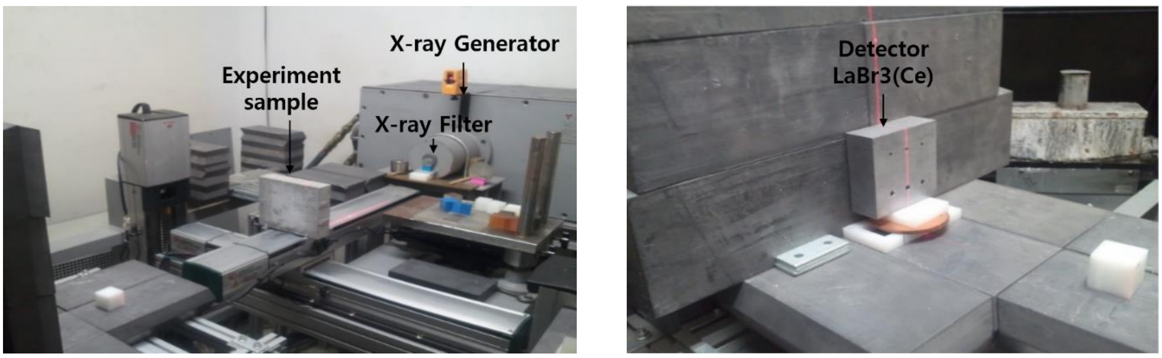

Figure 3. Experimental configuration for X-ray attenuation measurements

 doi: 10.20944/preprints201610.0006.v1

Table 4. X-ray generator

Manufacturer	Model	Main Specifications
Xylon	Power Generator, Plus & Minus Generator MG 452	Up 450kVp, X-ray irradiation up to 10mA
Xylon	Bipolar Metal-ceramic X-ray Tube YTU 450 -D02	Bipolar system of tubes. Stable high voltage irradiation possible.

Figure 4 shows the high-intensity γ-ray irradiation device used for the γ-ray irradiation experiment, and 1.17 and 1.33 MeV γ-rays emitted from a Co-60 radioactive isotope were used. Specimens identical to those used in the X-ray irradiation experiment were used, and the absorbed radiation dose was measured by analyzing the chemical change through chemical dosimetry. An alanine dosimeter was used in this study, which generates free radicals when it absorbs radiation, allowing the measurement of radiation dose using electron paramagnetic resonance (EPR).

Figure 4. Experimental configuration for gamma-ray attenuation measurements

This section may be divided by subheadings. It should provide a concise and precise description of the experimental results, their interpretation as well as the experimental conclusions that can be drawn.

3. Results

3.1 Slump test and Air content and Unit volume weight

Experimental results, including air content and slump test of each specimen, unit volume weight of fresh and hardened concretes, are shown in Table 5. Although the air content experiment showed a difference in air content owing to an arbitrary increase in the admixture mix at 40M (W/C ratio of 0.4 of magnetite mixed concrete) and 45M (W/C ratio of 0.45 of magnetite mixed concrete), all satisfied the air content allowance of 2.5–4.5 %.

The slump was found to be around 150 ± 25 mm, and the unit volume weights of each specimen show differences with weight ratio.

The unit volume weight experiment results revealed 3.11–3.21 t/m^3 of EAF, and magnetite, 45E(1)M(Ir10%), and 45E(1)(Ir40%) all satisfied the reference level of 3.4 t/m^3. W/C change did not entail any change in the unit volume weight.

Table 5. Test results of air content and unit volume weight of fresh and hardened concretes

Symbol of specimen	Slump	Air content	Predicted[1]	Experimental[2]	
			Unit volume weight	Fresh concrete	Hardened concrete
				Unit volume weight	Unit volume weight
	(mm)	(%)	(t/m^3)	(t/m^3)	(t/m^3)
40N	160	2.5	2.36	2.28	2.28
40E(1)	160	3.1	3.14	3.21	3.21
40M	155	4.0	3.65	3.47	3.55
40E(1)M	155	3.2	3.41	3.27	3.31
45N	170	3.0	2.38	2.34	2.34
45E(1)	160	3.1	3.10	3.11	3.11
45E(2)	165	3.2	2.87	2.91	2.91
45M	145	4.2	3.61	3.61	3.51
45E(1)M-Ir(10%)	155	3.4	3.59	3.50	3.30
45E(1)-Ir(40%)	155	3.5	3.63	3.65	3.45

[1] Calculated using the Equation (1); [2] ASTM C 173 standard based.

Figure 5 show a comparison of the predicted and measured unit volume weights of fresh and hardened concretes. Comparing the unit volume weights of concrete before and after hardening, at a W/C ratio of 0.4, the unit volume weights of 40M and 40E(1)M appeared to increase, and at a W/C ratio of 0.45, unit volume weights of 45M, 45E(1)M-Ir(10%), and 45E(1)-Ir(40%) appeared to decrease. It was observed that this difference occurs when the unit volume weight exceeds 3.27 t/m^3.

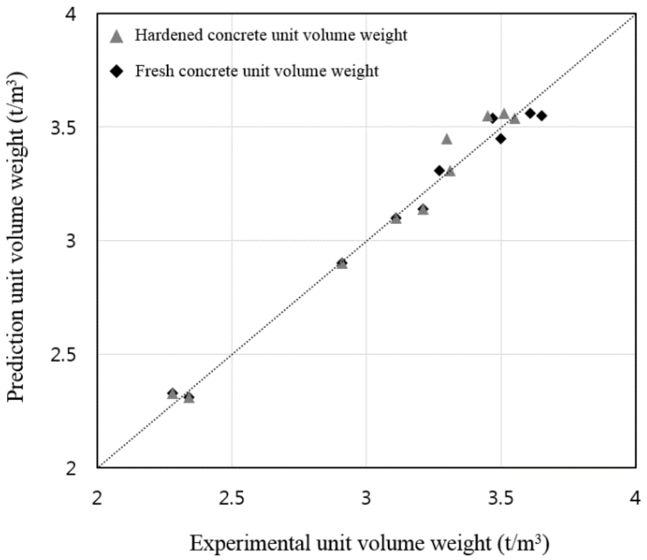

Figure 5. Compare the experimental unit volume weight with the predicted unit volume weight

3.2 Compressive strength test

The results of the compressive strength test at a W/C ratio showed 0.4. 40N exhibited the lowest compressive strength of 39.5 MPa. 40E(1) had a compressive strength of 60.2 MPa, and 40E(1)M showed the highest compressive strength of 61.5 MPa. EAF concrete demonstrated 20 MPa higher compared to normal concrete.

At w/c 45%, it resulted in 39.3 MPa which is the highest in 45E(1)-Ir(40%). In contrary, 45N was shown as the lowest at 39.3 MPa. Figure 6 shows the test results of compressive strength.

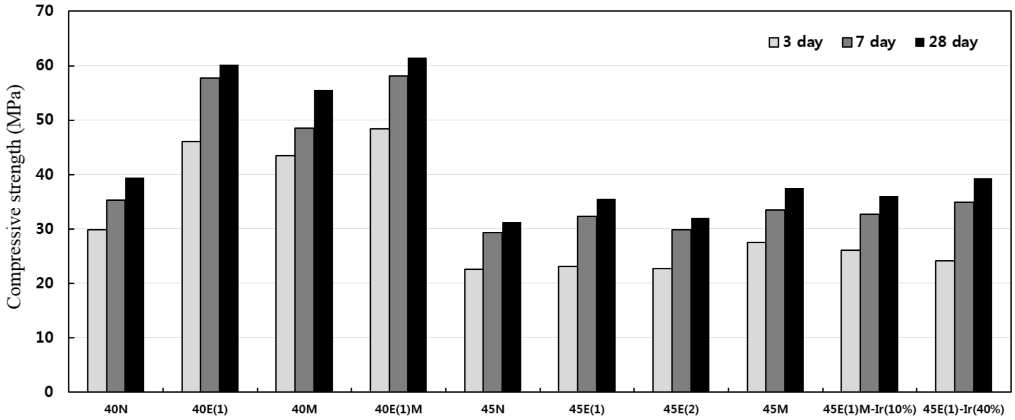

Figure 6. Test results of compressive strength

3.3 X-ray Irradiation Experiment

The fundamental equation for the X-ray irradiation experiment is Equation (6). Assume that the X-ray irradiating upon the shield has an intensity of I_0, while that after the irradiation can be denoted as I. Here, x is the thickness of the shield, and μ_t is the effective attenuation coefficient, which represents the probability of the X-ray causing an arbitrary interaction with the material per unit length. Linear attenuation coefficient can be described using the Lambert law.

$$I = I_O \cdot e^{-\mu_t \cdot x} \tag{6}$$

where, I = dose rate at the surface of the shield facing towards the X-ray source
I_0 = dose rate at the surface of the shield opposite to the X-ray source
μ_t = effective attenuation coefficient, which is a constant representing the X-ray absorption ratio of the shielding material.
x = thickness of the shield

Figure 7 shows the results of the X-ray irradiation experiment. The spectrum data of the source represents the default dose of X-ray in the absence of a shield. The spectrum data of the concretes using each material represents the X-ray shielding performance of the irradiated materials, with lower values of the data implying better shielding performance. The value of the data was the lowest at 40M, and the highest at 40N.

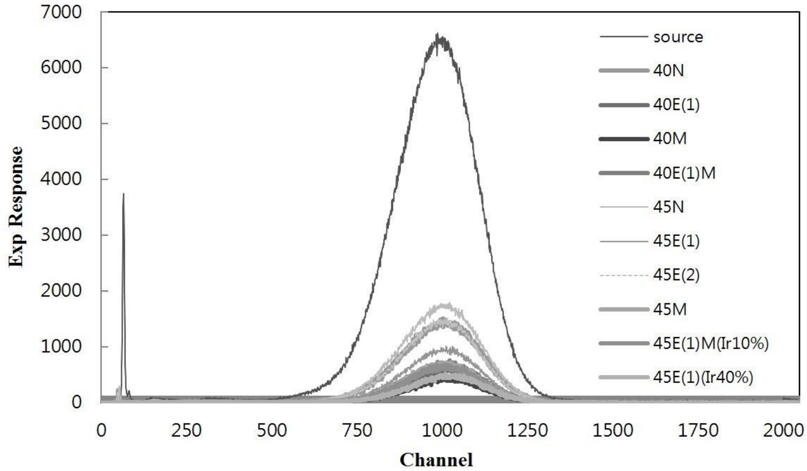

Figure 7. X-ray irradiation experiments

Table 6 shows the results from the X-ray shielding test. From the X-ray shielding ratio experiment, normal concrete specimens, 40N and 45N, showed a shielding ratio of around 73 %; EAF concretes, 40E(1), 45E(1) and 45E(2), showed a shielding ratio of around 88 – 91 %; EAF concretes containing iron powder, 45E(1)M-Ir(10%), 45E(1)-Ir(40%) had a shielding ratio of around 92-93 %; and magnetite concretes, 40M and 45M, showed a shielding ratio of around 93 %. Equivalent shielding effects are observed in 45E(1)M-Ir(10%) and 45E(1)-Ir(40%), of which the unit volume weight was discretionarily increased, and in magnetite concretes, 40M and 45M.

Table 6. Calculated data for the X-ray irradiation

Symbol of specimen	Unit volume weight	Spectrum Data	μt (cm^{-1})	Shielding rate (%)
Source		1,712,234	-	-
40N	2.28	450,588	0.267	73.68
40E(1)	3.21	148,117	0.490	91.35
40M	3.55	105,174	0.558	93.86
40E(1)M	3.31	127,588	0.519	92.55
45N	2.34	449,450	0.268	73.75
45E(1)	3.11	153,289	0.483	91.05
45E(2)	2.91	199,097	0.430	88.37
45M	3.51	114,073	0.542	93.34
45E(1)M-Ir(10%)	3.30	133,873	0.510	92.18
45E(1)-Ir(40%)	3.45	119,653	0.532	93.01

3.4 Gamma-ray Irradiation Experiment

The experimental results for the γ-ray irradiation experiment were obtained from chemical dosimetry using a γ-ray irradiation device. Table 7 shows the radiation dose and the shielding ratio measured after γ-ray irradiation. Although the shielding ratio appeared to be low since the strength of the γ-ray is high, with the thickness of the specimen being 5 cm, similar shielding effects are observed in EAF concrete, 40E(1), EAF concretes with discretionarily increased unit volume weight, 45E(1)M-Ir(10%) and 45E(1)-Ir(40%), and magnetite concretes, 40M and 45M.

Table 7. Results of the gamma-ray irradiation test

Symbol of specimen	Unit volume weight	Before (KGy)/h	After (KGy)/h	Shielding rate (%)
40N	2.28	0.51	0.35	31
40E(1)	3.21	0.50	0.32	37
40M	3.55	0.50	0.30	40
40E(1)M	3.31	0.50	0.31	38
45N	2.34	0.50	0.36	28
45E(1)	3.11	0.51	0.32	36
45E(2)	2.91	0.51	0.34	34
45M	3.51	0.51	0.31	40
45E(1)M-Ir(10%)	3.30	0.51	0.31	40
45E(1)-Ir(40%)	3.45	0.50	0.30	40

4. Discussion

Preprints (www.preprints.org) | NOT PEER-REVIEWED | Posted: 4 October 2016 doi: 10.20944/preprints201610.0006.v1

4.1 Properties of Concrete before and After Hardening

Figure 8 shows the experimental results for the unit volume weight and compressive strength of hardened concrete. There was no significant difference in unit volume weights of the specimens with W/C ratios of 0.4 and 0.45. Comparing the unit volume weights and compressive strengths of each specimen, it was found that the compressive strength increases with unit volume weight. However, when the unit volume weight was greater than 3.27 t/m³, a decrease in strength was also observed.

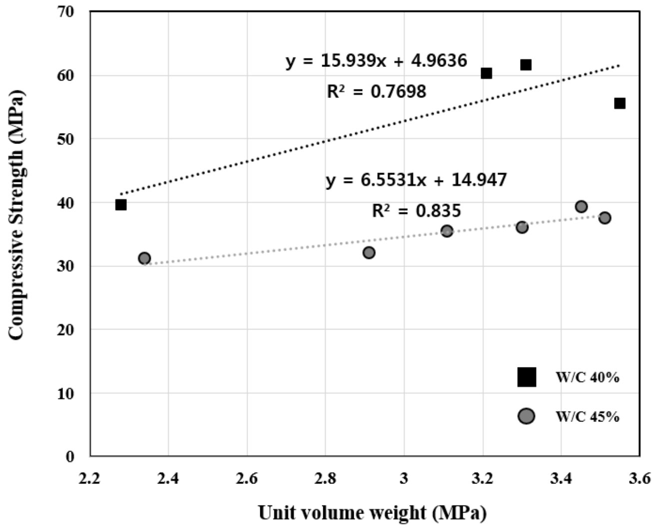

Figure 8. Test results of unit volume weight and compressive strength

4.2 X-ray Shielding Performance

Figure 9 shows the effective attenuation coefficient against the unit volume weight and shielding ratio. It can be seen that the effective attenuation coefficient increases with unit volume weight, and the correlation of the increase in shielding rate with increasing unit volume weight is shown. If the unit volume weight of the concrete is high, the effective attenuation coefficient can be seen that the increase in the shielding ratio is followed accordingly.

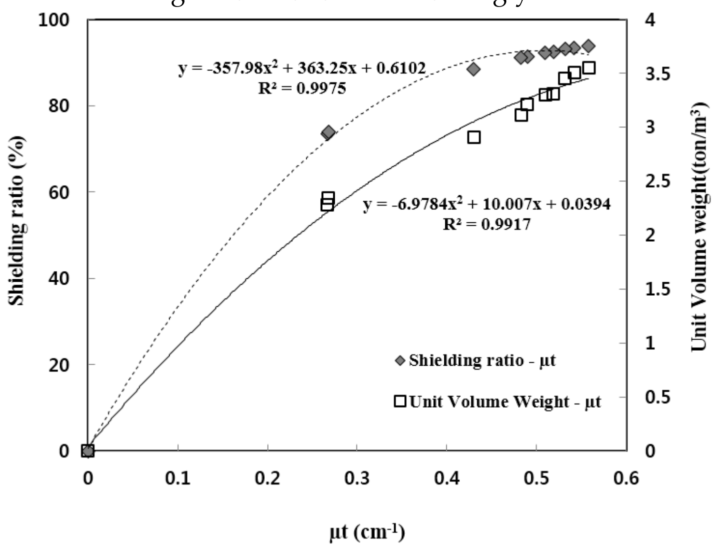

Figure 9. Unit volume weight - μt – Shielding rate Correlations

Figure 10 shows an analysis of shielding ratio with respect to shield thickness and unit volume weight. It shows the change of thickness by using the equation (6) to fixing the effective attenuation coefficient. With a unit volume weight of over 3.0 t/m³, the shielding ratio was 99 % for a thickness of

 doi: 10.20944/preprints201610.0006.v1

20 cm; in contrast, for normal concretes, the shielding ratio was 99 % for a thickness of 30 cm. It can be observed that the thickness of the concrete decreases as the unit volume weight increases.

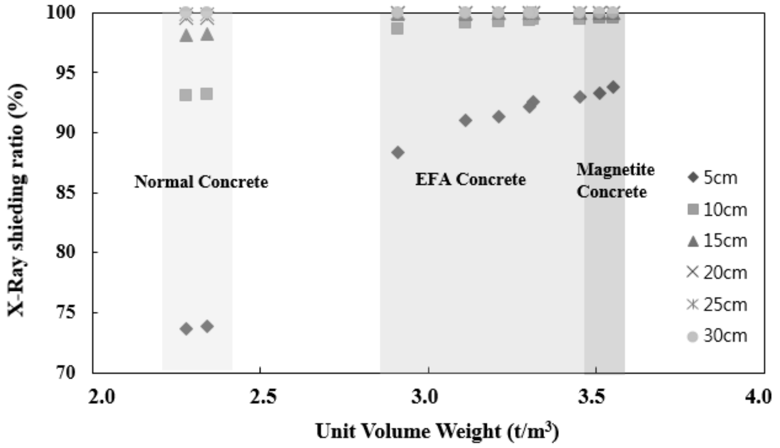

Figure 10. Unit volume weight and X-ray shielding rate Correlations

4.3 Gamma-ray Shielding Performance

While no significant difference can be observed in the shielding ratios of each concrete due to the high penetration ratio of γ rays, it can be observed that the γ-ray shielding ratio increases with unit volume weight, with a trend similar to the case for X-ray irradiation.

Figure 11 shows the results for gamma-ray shielding ratio. The shielding ratio is up to 40% for a thickness of 5 cm. Normal concretes, 40M and 45M, show a 99 % shielding ratio at a thickness of around 60 cm. EAF concretes, 40E(1) and 45E(1) show a stable shielding ratio at a thickness of 45-50 cm, and EAF concretes with discretionarily increased unit volume weight, 45E(1)M-Ir(10%) and 45E(1)-Ir(40%), and magnetite concretes, 40M and 45M, show a stable shielding ratio at a thickness of 40-45 cm.

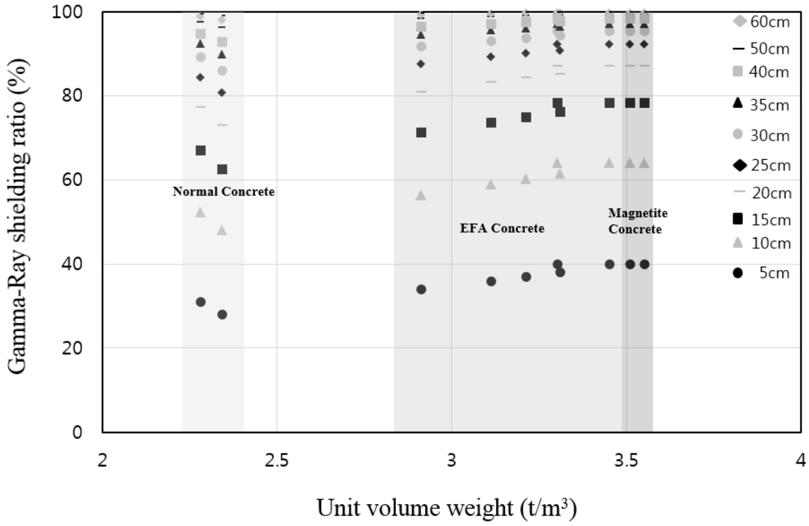

Figure 11. Unit volume weight and radiation shielding rate Correlations

5. Conclusions

The following results were obtained from the experimental evaluation of the applicability of EAF as a radiation shielding concrete.

- Unit volume weights of magnetite, EAF, EAF with iron powder, and normal aggregate concretes were observed to be 3.50 t/m³, 3.20 t/m³, 3.45 t/m³, and 2.30 t/m³ respectively. While

EAF concrete possesses a lower density than magnetite concrete, it satisfies the standard used in previous works if iron powder is added.

- EAF concrete showed a higher compressive strength than magnetite concrete, and an excellent liquidity during mixing. While the compressive strength of the concrete increases with unit volume weight, magnetite does not exhibit sufficient strength due to the separation of ingredients during mixing, as the density of magnetite is high.
- From the X-ray irradiation experiment, the shielding ratios of magnetite, EAF, EAF with iron powder, and normal aggregate concretes were determined to be 93.9 %, 91.2 %, 93 %, and 73.7 % respectively, indicating a linear relationship with unit volume weight.
- In terms of X-ray shielding ratio, it was observed that around 20 cm thickness was necessary to ensure sufficient radiation shielding with normal concretes, while a thickness of 10–15 cm was required to achieve similar shielding ratio for EAF concrete. Moreover, in terms of γ-ray shielding ratio, a 99 % shielding ratio was obtained for normal concretes with a thickness of 60 cm. EAF concretes, 40E(1) and 45E(1) showed a stable shielding ratio at a thickness of 45-50 cm, and EAF concretes with discretionarily increased unit volume weight, 45E(1)M-Ir(10%) and 45E(1)-Ir(40%), and magnetite concretes, 40M and 45M showed a stable shielding ratio at a thickness of 40-45 cm.
- Comparing the X-ray and γ-ray shielding ratios, similar linear relationships were observed. It was found that EAF concrete can be used as a radiation shielding concrete, and a superior performance to magnetite concrete was obtained in terms of strength and slump.
- The biggest problem of magnetite concrete is segregation of aggregates and poor moldability when the concrete is cast. However, it was confirmed that EAF concrete has great abilities to fluidity, strength and the performance of radiation shield. When EAF concrete is employed to buildings using X-ray and γ-ray, it is decided that construct ability will be retained due to the reduction of wall thickness and EAF concrete, which is considered as one of the by-products, will be used as higher value-added. This finding favored the feasibility of the development of radiation-shielding concrete using electric arc furnace oxidizing slag aggregates.

Acknowledgments: This research was supported by Basic Science Research Program through the National Research Foundation of Korea (NRF) funded by the Ministry of Science, ICT & Future Planning (No.2015R1A5A1037548)

Author Contributions: Han-Seung Lee planned and managed the project. Hee-Seob Lim conducted the experiments, analyzed the data, and compiled the final manuscript. Moreover, all authors reviewed the data and the final manuscript.

Conflicts of Interest: The authors declare no conflict of interest.

References

1. Pomaro, B.; Salononi, V.A.; Gramegna, F.; Prete, G.; Majorana, C.E. Radiation damage evaluation on concrete within a facility for selective production of exotic species (SPES project), Italy. J. Hazad. Mater. **2011**, *194*, 169-177.
2. Gencel, O. Effect of elevated temperatures on mechanical properties of high-strength concrete containing varying proportions of hematite, Fire. Mater. **2012**, *36*, 217-230.
3. Chitralekha; Kerur, B.R.; Lagare, M.T.; Nathuram, R.; Sharma, D.N. Mass attenuation coefficients of saccharides for low-energy X-rays, Radiat. Phys. Chem. **2005**, *72*, 1-5.
4. El-Khayatt, A.M. Radiation shielding of concretes containing different lime/silica ratios, Ann. Nucl. Energy **2010**, *37*, 991-995.
5. Agosteo, S.; Magistris, M.; Mereghetti, A.; Silari, M.; Zajacova, Z. Shielding data for 100-250 MeV proton accelerators: Attenuation of secondary radiation in thick iron and concrete/iron shields, Nucl. Instrum. Methods Phys. Res. B. **2008**, *266*, 3406-3416.
6. ACI 304R Guide for Measuring, Mixing, Transporting and Placing Concrete.
7. Xi, S.; Bourham, M.; Rabiei, A. A novel ultra-light structure for radiation shielding, Mater. Des. **2010**, *31*, 2140-2146.

 doi: 10.20944/preprints201610.0006.v1

8. Akkurt, I.; Basyigit, C.; Kilincarslan, S.; Mavi, B.; Akkurt, A. Radiation shielding of concretes containing different aggregates, Cem. Concr. Compos. **2006**, *28*, 153- 157.
9. Kharita, M.H.; Takeyeddin, M.; Alnassar, M.; Yousef, S. Development of special radiation shielding concretes using natural local materials and evaluation of their shielding characteristics, Prog. Nucl. Energy. **2008**, *50*, 33-36.
10. Akkurt, I.; Akyildirim, H.; Mavi, B.; Kilincarslan, S.; Basyigit, C. Photon attenuation coefficients of concrete includes barite in different rate, Ann. Nucl. Energy. **2010**, *37*, 910-914.
11. Mesbahi, A.; Azarpeyvand, A.; Shirazi, A. Photoneutron and backscattering in high density concretes used for radiation therapy shielding, Ann. Nucl. Energy. **2011**, *38*, 2752-2756.
12. Maslehuddin, M.; Naqvi, A.A.; Ibrahim, M.; Kalakada, Z. Radiation shielding properties of concrete with electric arc furnace slag aggregates and steel shots, Ann. Nucl. Energy. **2013**, *53*, 192-196.
13. Akkurt, I.; Akyildirim, H.; Mavi, B.; Kilincarslan, S.; Basyigit, C. Gamma-ray shielding properties of concrete including barite at different energies, Prog. Nucl. Energy. **2010**, *52*, 620-623.
14. Rezaei Ochbelagh, D.; Azim Khani, S.; Gasemzadeh Mosavinejad, H. Effect of gamma and lead as an additive material on the resistance and strength of concrete, Nucl. Eng. Des. **2011**, *241*, 2359-2363.
15. Sharma, A.; Reddy, G.R.; Varshney, L.; Bharathkumar, H.; Vaze, K.K.; Ghosh, A.K; Kushwaha, H.S.; Krishnamoorthy, T.S. Experimental investigations on mechanical and radiation shielding properties of hybrid lead-steel fiber reinforced concrete, Nucl. Eng. Des. **2009**, *239*, 1180-1185.
16. Turkmen, I.; Ozdemir, Y.; Kurudirek, M.; Demir, F.; Simsek, O. Calculation of radiation attenuation coefficients in portland cements mixed with silica fume, blast furnace slag and natural zeolite, Ann. Nucl. Energy. **2008**, *35*, 1937–1943.
17. Singh, C.; Singh, T.; Kumar, A.; Mudahar, G.S. Energy and chemical composition dependence of mass attenuation coefficients of building materials, Ann. Nucl. Energy. **2004**, *31*, 1199–1205.
18. Alam, M.N.; Miah, M.M.H.; Chowdhury, M.I.; Kamal, M.; Ghose, S.; Rahman, R. Attenuation coefficients of soils and some building materials of Bangladesh in the energy range 276-1332 keV, Appl. Radiat. Isot. **2001**, *54*, 973–976.
19. Salinas, I.C.P.; Conti, C.C.; Lopes, R.T. Effective density and mass attenuation coefficient for building material in Brazil, Appl. Radiat. Isot. **2006**, *64*, 13-18.
20. Medhat, M.E. Gamma-ray attenuation coefficients of some building materials available in Egypt, Ann. Nucl. Energy. **2009**, *36*, 849-852.
21. Faraone, N.; Tonello, G.; Furlani, E.; Maschio, S. Steelmaking slag as aggregate for mortars: Effects of particle dimension on compression strength, Chemosphere. **2009**, *77*, 1152-1156.
22. Qasrawi, H.; Shalabi, F.; Asi, I. Use of low CaO unprocessed steel slag in concrete as fine aggregate. Constr, Build. Mater. **2009**, *23*, 1118-1125.
23. Correia, S.L.; Souza, F.L.; Dienstmann, G.; Segadaes, A.M. Assessment of the recycling potential of fresh concrete waste using a factorial design of experiments, Waste Manage. **2009**, *29*, 2886-2891.
24. Salihoglu, G.; Pinarli, V. Steel foundry electric arc furnace dust management: Stabilization by using lime and portland cement, J.Hazad. Mater. **2008**, *153*, 1110-1116.
25. Wang, G.; Wang, Y.; Gao, Z. Use of steel slag as a granular material: Volume expansion prediction and usability criteria, J. Hazad. Mater. **2010**, *184*, 555-560.
26. Wang, G. Determination of the expansion force of coarse steel slag aggregate, Constr. Build. Mater. **2010**, *24*, 1961-1966.
27. Adegoloye, G.; Beaucour, A.L.; Ortola, S.; Noumowe, A. Concretes made of EAF slag and AOD slag aggregates from stainless steel process: Mechanical properties and durability, Constr. Build. Mater. **2015**, *76*, 313-321.
28. Roslan, N.H.; Ismail, M.; Abdul-Majid, Z.; Ghoreishiamiri, S. Performance of steel slag and steel sludge in concrete, Constr. Build. Mater. **2016**, *104*, 16-24.
29. ASTM C 33 Standard Specification for Concrete Aggregates.
30. ASTM C 29 Standard Test Method for unit weight and voids in Aggregate.
31. ASTM C 127 Test Method for Relative Density(Specific Gravity) and Absorption of coarse aggregate.
32. ASTM C 128 Test Method for Relative Density(Specific Gravity) and Absorption of Fine Aggregate.
33. ASTM C 136 Standard Test Method for sieve Analysis of Fine and Coarse Aggregates.
34. ASTM C 150-05 Standard specification for Portland cement.
35. ASTM C 173 Standard Test Method for Air Content of Freshly Mixed Concrete by the Volumetric Method.

 doi: 10.20944/preprints201610.0006.v1

36. ASTM C 143 Standard Test Method for Slump of Hydraulic-Cement Concrete.
37. ASTM C 39 Standard Test Method for Compressive Strength of Cylindrical Concrete Specimens.